AD-A141 927 KINETIC PROCESSES IN HIGH PRESSURE GASES EXCITED STATE COLLISIONS(U) MISSOURI UNIV-ROLLA DEPT OF PHYSICS L D SCHEARER DEC 83 TR-14 N00014-75-C-0477 1/1

UNCLASSIFIED F/G 7/4 NL

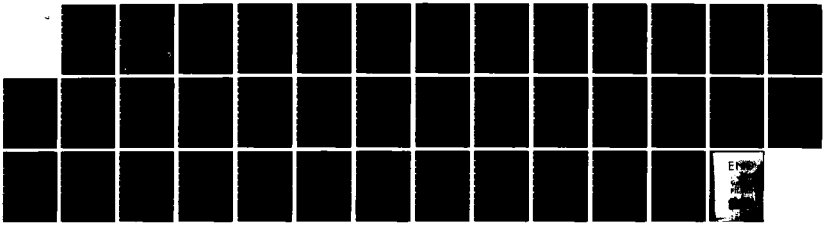

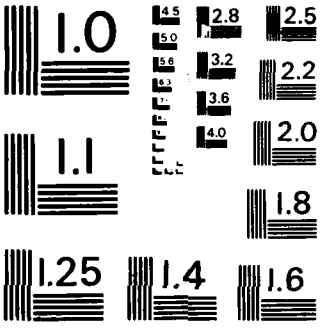

MICROCOPY RESOLUTION TEST CHART
NATIONAL BUREAU OF STANDARDS - 1963 - A

AD-A141 927

DTIC FILE COPY

84 06 07 052

Unclassified

SECURITY CLASSIFICATION OF THIS PAGE *(When Data Entered)*

REPORT DOCUMENTATION PAGE		READ INSTRUCTIONS BEFORE COMPLETING FORM
1. REPORT NUMBER 14	2. GOVT ACCESSION NO. AD-A142 927	3. RECIPIENT'S CATALOG NUMBER
4. TITLE *(and Subtitle)* Kinetic Processes in High Pressure Gases: Excited State Collisions		5. TYPE OF REPORT & PERIOD COVERED Technical Report-Final 1 Jan '82 - 31 Mar '83
		6. PERFORMING ORG. REPORT NUMBER
7. AUTHOR(s) L. D. Schearer		8. CONTRACT OR GRANT NUMBER(s) ONR N00014-75C-0477
9. PERFORMING ORGANIZATION NAME AND ADDRESS The Curators of the University of Missouri for the University of Missouri-Rolla, Rolla, MO 65401		10. PROGRAM ELEMENT, PROJECT, TASK AREA & WORK UNIT NUMBERS NR 343 011
11. CONTROLLING OFFICE NAME AND ADDRESS Department of the Navy Office of Naval Research Washington, D.C. 20360		12. REPORT DATE Dec 1983
		13. NUMBER OF PAGES
14. MONITORING AGENCY NAME & ADDRESS(if different from Controlling Office)		15. SECURITY CLASS. (of this report) Unclassified
		15a. DECLASSIFICATION DOWNGRADING SCHEDULE

16. DISTRIBUTION STATEMENT *(of this Report)*

Approved for public release: Distribution unlimited.

17. DISTRIBUTION STATEMENT *(of the abstract entered in Block 20, if different from Report)*

18. SUPPLEMENTARY NOTES

19. KEY WORDS *(Continue on reverse side if necessary and identify by block number)*

line shifts, line broadening, recombination, Rydberg atoms, sodium vapor, multi-photon ionization.

20. ABSTRACT *(Continue on reverse side if necessary and identify by block number)*

Spectral line shifts for 3P-nD transitions in sodium induced by collisions with helium, argon, and krypton for n=5 to 18 have been measured. The line shifts of the diffuse series transitions increase rapidly with principal quantum number and asymptotically approach the limit predicted by the Fermi model at high quantum numbers.

DD FORM 1 JAN 73 1473 EDITION OF 1 NOV 65 IS OBSOLETE
S/N 0102-LF-014-6601

SECURITY CLASSIFICATION OF THIS PAGE *(When Data Entered)*

TECHNICAL REPORT

FINAL

KINETIC PROCESSES IN HIGH PRESSURE GASES: EXCITED STATE COLLISIONS

L. D. Schearer

Department of Physics

University of Missouri-Rolla

Rolla, MO 65401

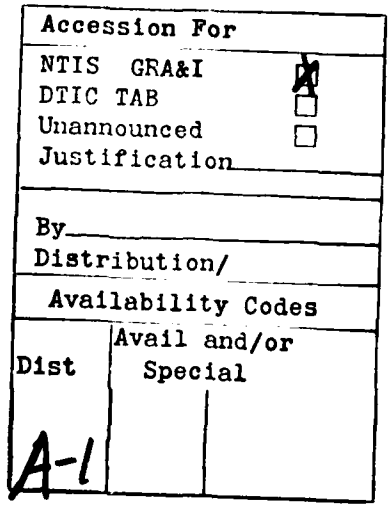

Technical Report to the Office of Naval Research.
Grant No. N00014-75-C-0477 for the period Jan 1982 - Apr 1983.

CONTRACT DESCRIPTION

The purpose of the research program is to investigate energy exchange and energy loss mechanisms in discharge plasmas and their afterglows. Specific mechanisms which have been investigated in our laboratory include: (a) metastable interactions, such as dissociative excitation and Penning ionization, (b) collisional broadening and level shifts in excited states produced by the presence of a buffer gas and/or electrons, and (c) electron loss mechanisms due to volume recombination.

I. INTRODUCTION

This research program deals with the kinetic and radiative processes occurring in a dense mixture of alkali vapor and a noble gas buffer which has been excited by short, powerful laser pulses.

A variety of devices, including atmospheric pressure lasers, high current/low inductance switches, high efficiency lamps, and inertial confinement fusion targets utilize similar, excited atomic vapors at high pressures. With the current interest in these devices, the role of collisional and radiative processes involving highly excited (Rydberg) states has taken on a new importance. A common feature of all these devices is that energy is deposited into the system in the form of large densities of ion/electrons, metastable species, and various excited neutrals. This energy is then transferred to some desired channel; e.g., a lasing transition, electron production, electron heating, etc. The efficiency of this energy transfer and, indeed, the efficiency of the initial excitation process, depend on the specific collisional and radiative processes occurring in the mixture. For instance, radiation loss depends strongly on the degree of radiation trapping, which in turn, depends on the collisional linewidths and shifts of the transitions involved.

The general experimental approach of this work consists of exciting the mixture in a time short compared to the time in which the system relaxes. The behavior of a freely relaxing system may then be related to the fundamental processes occurring in the system. This is the rationale behind our earlier conventional afterglow experiments which have yielded a great deal of information regarding the behavior of gaseous discharges at

lower pressures.

The present work differs from conventional afterglow experiments in that the latter use some form of microwave or radio frequency breakdown as the source of excitation, whereas this work uses optical frequency (laser) excitation. The absorption of optical energy from high power laser pulses may be well characterized, and therefore the initial conditions of the excited vapor are well known. In contrast, microwave and radio frequency breakdown are typically stochastic and the initial conditions of the excited system varies substantially from pulse to pulse. Furthermore, microwave and radio frequency breakdown is difficult to achieve at the high pressures with which this study is concerned.

II. PROGRESS REPORT

Kinetic processes in Na + R.G. mixtures have been examined for rare gas densities between 400 and 2000 Torr and Na densities up to 1 Torr. Electron/ion densities up to 10^{15} cm^{-3} are obtained under typical experimental conditions.

We have measured excitation rates for Na(3p) + Na(3p) → Na(4,5,6d n 6s) + Na(3s) collisions, spectral line shifts due to buffer gas collisions and stark shifts due to electron collisions, and electron densities and electron temperatures in the afterglow of high power laser pulses. This final contract period concentrated on spectral line shifts in Na due to collisions with Ar, He, and Kr.

A number of interesting effects occur when a dense sodium vapor is excited by laser radiation tuned to one of the D lines. In particular, (1) complete ionization has been observed when high power, pulse lasers are employed[1] and (2) surprisingly high densities of atoms are observed in the nd (n=3,4,5) and ns (n=5,6) levels when a CW laser is employed[2].

Theoretical calculations[3] indicate that the ionization present in the first case is due to electron heating via superelastic collisions followed by electron impact ionization. A small initial number of electrons (seed electrons) is supplied by several, comparatively weak mechanisms including associative ionization and two photon ionization of the 3p state atoms.

In order to observe these effects on a time resolved basis, we used short (4 ns) laser pulses to excite the 3p states and create the initial electron density. The experimental arrangement is shown in Fig. 1. Kopystynska and Kowalczyk[4] had earlier used short laser pulses to excite

the D lines and observe subsequent radiative emission from excited nd and ns states; however, they made no attempt to independently vary the seed electron concentration by using a second ionizing laser pulse as is described in this experiment.

THREE PHOTON ABSORPTION PROCESSES

The optical emission from the ionized volume at times greater than 0.5 μs after the laser pulse results from collisional-radiative recombination processes. If one integrates this emission signal over all times and over all wavelengths, the number of photons collected is proportional to the total number of ion-electrons formed in the excitation-ionization process.

If a second (blue) laser is tuned through a 3p-nd (ns) transition, the number of "seed" electrons produced is proportional to the transition moment, the laser intensity, and the photoionization cross section of the nd (ns) state. The "seed" electron density in turn determines the ultimate ion/electron density. If we observe the integrated emission from the interaction zone and scan the frequency of the second laser, we obtain the spectrum shown in Fig. 2. Since the excitation of the nd (ns) excited state takes place only during the 4 ns laser pulse, well before the ion/electron density reaches its peak, the shift of the spectral lines as observed while tuning the blue laser through a transition is *due only to the presence of the buffer gas.*

Line Shifts. One can deconvolute the wavelength dependence of the ion yield and obtain the line width of the 3p-nd transitions. Because the line width parameters for these transitions have recently been measured using a photon echo technique, it was decided to concentrate on the line shifts which cannot be measured by photon echo techniques. Providing the laser bandwidth is significantly narrower than the bandwidth of the resonant transition, the wavelength of maximum ionization corresponds to the maximum of the line shape function. The maximum of the line shape

function defines the line center, even for an asymmetric profile. Thus, it was possible to measure the line shifts without resorting to a detailed deconvolution of the resonance ionization spectra.

In order to attain a sufficiently narrow bandwidth from the photoionizing dye laser, the laser was modified by insertion of a 25X telescope in the laser cavity in place of the standard 10X telescope. The bandwidth of the modified laser was measured with a 1m grating monochromator in the third order and found to be 0.15 Å compared with the standard bandwidth of 0.4 Å. In all measurements, the apparent width of the line profile was at least a factor of four greater than the laser bandwidth, so that any error in measuring the line center due to the finite bandwidth of the laser was small.

Figure 1 is a schematic of the apparatus used to determine the line shifts. Following an optical delay of 8 ns, the output of the ionizing laser was combined using a 50 percent transmitting beam splitting mirror with the output from the laser tuned to the 3s-3p transition. The result was a superposition of the two monochromatic beams to form two di-chromatic beams. One of the resulting di-chromatic beams was directed to a cell containing sodium and approximately 0.5 amagats of noble buffer gas. One beam was directed to a cell containing sodium with no buffer. The resonance ionization signals from both cells were recorded simultaneously by the computer as the wavelength drive of the photoionizing laser is advanced across the transition. Figure 2 is a scan of ion yield versus laser wavelength taken for the high pressure cell over a broad range of laser wavelength. Figure 3 is a typical scan showing the resonance ionization signal from both cells as they were recorded simultaneously by the computer. The scan is a doublet in the

high pressure cell due to collisional mixing of the $3^2p_{3/2,1/2}$ levels by the rare gas atoms. In the low pressure cell, this mixing does not occur and therefore only one resonance is recorded.

The ion yield in the low pressure reference cell was monitored directly by collecting the ions and electrons at appropriately biased parallel plates. The resulting current pulse in the load resistor was a direct measure of the number of ions produced, provided that space charge effects at the plates, Debye shielding effects in the production region, and gas breakdown are avoided. To prevent these difficulties, the cell was typically operated at a temperature less than 250°C and the collection voltage was maintained at less than 10 v/cm. By operating the cell at such a low temperature the ion density was no more than $10^8 cm^{-3}$ implying an initial Debye shielding length of about 0.1 cm and hence the absence of space charge effects in the production region or at the collection plates. The load resistance was typically 20 KΩ. The relative charge per pulse flowing through the load resistor was measured by integrating the voltage across the load resistor during a time window larger than the duration of the current pulse:

$$Q_{pulse} = \int_o^{t>>\tau'} I(t)\, dt$$

$$= \frac{1}{R_L} \int_o^{t>>\tau'} V(t)\, dt$$

where τ' = signal pulse length.

This was accomplished using a PAR 160 boxcar integrator in the fixed delay mode, which permitted an adjustable degree of signal averaging over several laser pulses.

The ion yield in the high pressure cell was monitored by observing the

total recombination signal on a strong, low lying atomic transition. This is a measure of the relative ion yield. Because of the long, slow decay of the fluorescence, it was advantageous to use photon counting techniques in recording the recombination fluorescence. The principal advantage of photon counting is the suppression of noise by not counting pulses below a certain magnitude fixed by the discriminator. Since the pulse height distribution of noise pulses (also called "dark count pulses") is weighted toward lower magnitudes relative to the pulse height distribution of signal pulses, photon counting improves the signal to noise ratio over simple tube current measurements. A limitation of photon counting is saturation of the signal at high count rates. This occurs when the average time between photon pulses becomes such that the counter has insufficient time to recover between counts. The SSR 1110 photon counter has a rated pulse pair resolution of 12 ns, which permits linear intensity measurements up to about 20 photons per microsecond. Experimentally, the recombination emission photon count was observed to depart from linearity at about 100 counts per laser shot as tested with calibrated neutral density filters. This is approximately the behavior anticipated considering the decay time of the recombination emission (see Figure 3). Relative ion yield data was always taken at count rates corresponding to less than 100 counts per laser shot.

Figures 4, 5, and 6 show the measured line shift parameters for the $3^2P - n^2D$ transitions with argon, krypton and helium perturbers respectively. Also shown in Figure 4 are the shifts calculated using the Lindholm-Foley[5] approximation, which is the impact limit of Anderson theory[6]. It is seen that for argon, the Lindholm-Foley approximation departs sharply from experiment for levels above about n = 6. This is

to be expected since the impact approximation assumes that the time between collisions is much greater than the duration of collisions. At n = 7 in argon the time between collisions, τ, is:

$$\tau \simeq \frac{1}{n \sigma \langle v \rangle} \sim 10^{-11} \text{ sec}$$

while the duration of collision is about $\tau_c \sim 10^{-12}$ sec.

Also shown in Figures 4, 5, and 6 are the predictions of the Fermi model[7], with polarization corrections, and results from previous work on the principal series transitions. The principal series transitions are seen to be more strongly shifted at low quantum number than are the diffuse series transitions, but approach the same limit at high quantum number.

CONCLUSIONS

Following the investment of a substantial amount of energy in the saturation of the resonance transition, the evolution of the system divides itself into two distinct time domains. The first time domain extends over the trapped lifetime of the resonance transition during which most of the energy of the system is stored in the large population of excited Na(3p) atoms. The second domain extends over the recombination time for the Na^+ ions, during which most of the energy of the system is associated with ionization. Within the trapped lifetime of the Na(3p) resonance state, substantial populations of atoms are found in levels with energies roughly twice the energy of the Na(3p) atoms. A second laser tuned to the photoionization threshold of the Na(3p) atoms produces appreciable ionization. Enhancement of the ionization by electron impact excitation is observed. While a large concentration of Na(3p) atoms is present, a transfer of some population to higher energy levels, including the continuum, occurs via electron impact collisions and excitation transfer collisions. The electron impact process dominates collisional ionization, while excitation transfer collisions appear to dominate the loss to higher energy levels. The measured rate constant for excitation transfer to the Na(4d) level was found to agree roughly with the value calculated by Kowalczyk. For other levels, the decline in excitation transfer rate constant with energy level was found to follow approximately the reduction in the fraction of atoms in a Boltzmann distribution with kinetic energies greater than the energy defect.

Once the large density of Na(3p) atoms has radiatively decayed, the principal reservoir of energy is the population of ions and free electrons.

This is the second time domain of the afterglow. Recombination occurs on a many-microsecond time scale. No evidence of dissociative or neutral stabilized recombination is observed. The dominant energy loss mechanism is atomic line emission.

The shift of atomic energy levels due to the presence of the high density of buffer atoms is found to agree well with the Lindholm-Foley approximation of Anderson theory at low principal quantum number and with the Fermi limit at high quantum number. This work shows, for the first time, that the diffuse series transitions approach the same limit for their shifts at high quantum number as do the principal series transitions. While this result is expected based on Fermi's analysis, and the equality of the Fermi limit for the principal series of different alkali atoms has been experimentally established, the equality for different angular momentum states further validates the correctness of the theory.

REFERENCES

1. (a) T. B. Lucatorto and T. J. McIlrath, Phys Rev Lttt, 37 428 (1976);
   (b) T. J. McIlrath and T. B. Lucatorto, ibid, 38 1390 (1977).

2. M. Allegrini, G. Alzetta, A. Kopystynska, L. Moi and G. Orriols, Opt. Common, 19, 96 (1976).

3. R. M. Measures and P. T. Cardinal, Phys. Rev. A, 23, 804 (1981).

4. A. Kopystynska and P. Kowalczyk, Opt. Commun., 25, 351 (1978).

5. H. M. Foley, Phys. Rev. 69, 287 (1946).

6. P. W. Anderson, Phys. Rev. 76, 647 (1949).

7. E. Fermi, Nuovo Cimento 11, 15 (1934).

Figure Captions

Figure 1. Schematic of the apparatus.

Figure 2. Scan of ion yield versus the wavelength of the second, ionizing laser. The ionization limit corresponds to a wavelength of 408 nm.

Figure 3. Ion yield versus laser wavelength for the 3p → 8d transitions from a scan taken simultaneously in a cell with 400 torr of argon buffer and a cell with no buffer gas. Two components are present in the high pressure cell due to collisional mixing of the $3^2P_{3/2,\ 1/2}$ levels.

Figure 4. Spectral line shifts as a function of principal quantum number 3p - nd. Argon-Na at 400 Torr.

Figure 5. Spectral line shifts as a function of principal quantum number 3p - nd. Kr - Na at 400 Torr.

Figure 6. Spectral line shifts as a function of principal quantum number 3p - nd. He - Na at 400 Torr.

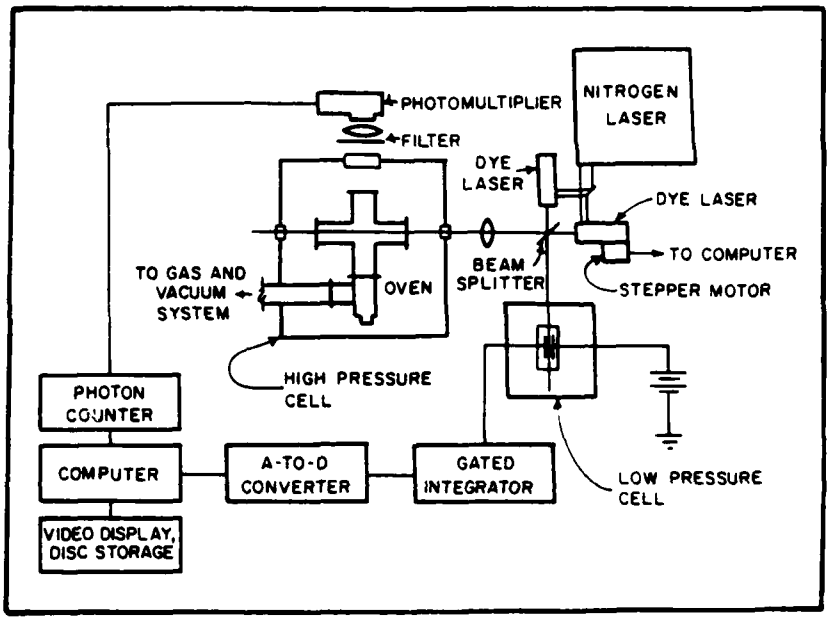

Figure 1. Schematic of the apparatus.

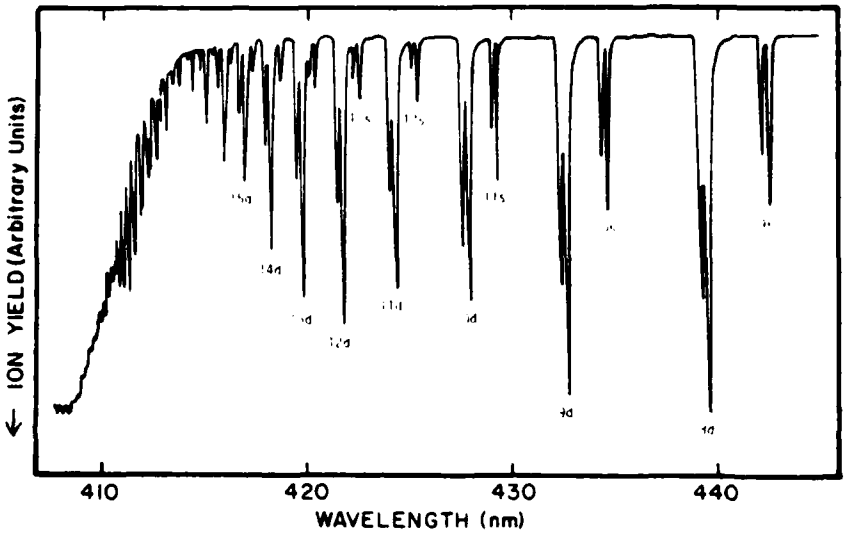

Figure 2. Scan of ion yield versus the wavelength of the second, ionizing laser. The ionization limit corresponds to a wavelength of 408 nm.

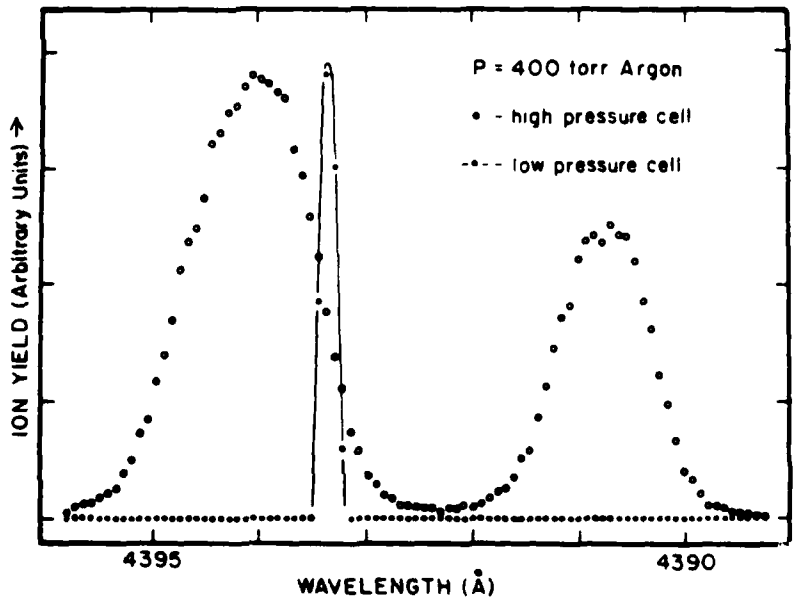

Figure 3. Ion yield versus laser wavelength for the 3p → 8d transitions from a scan taken simultaneously in a cell with 400 torr of argon buffer and a cell with no buffer gas. Two components are present in the high pressure cell due to collisional mixing of the $3^2P_{3/2,\ 1/2}$ levels.

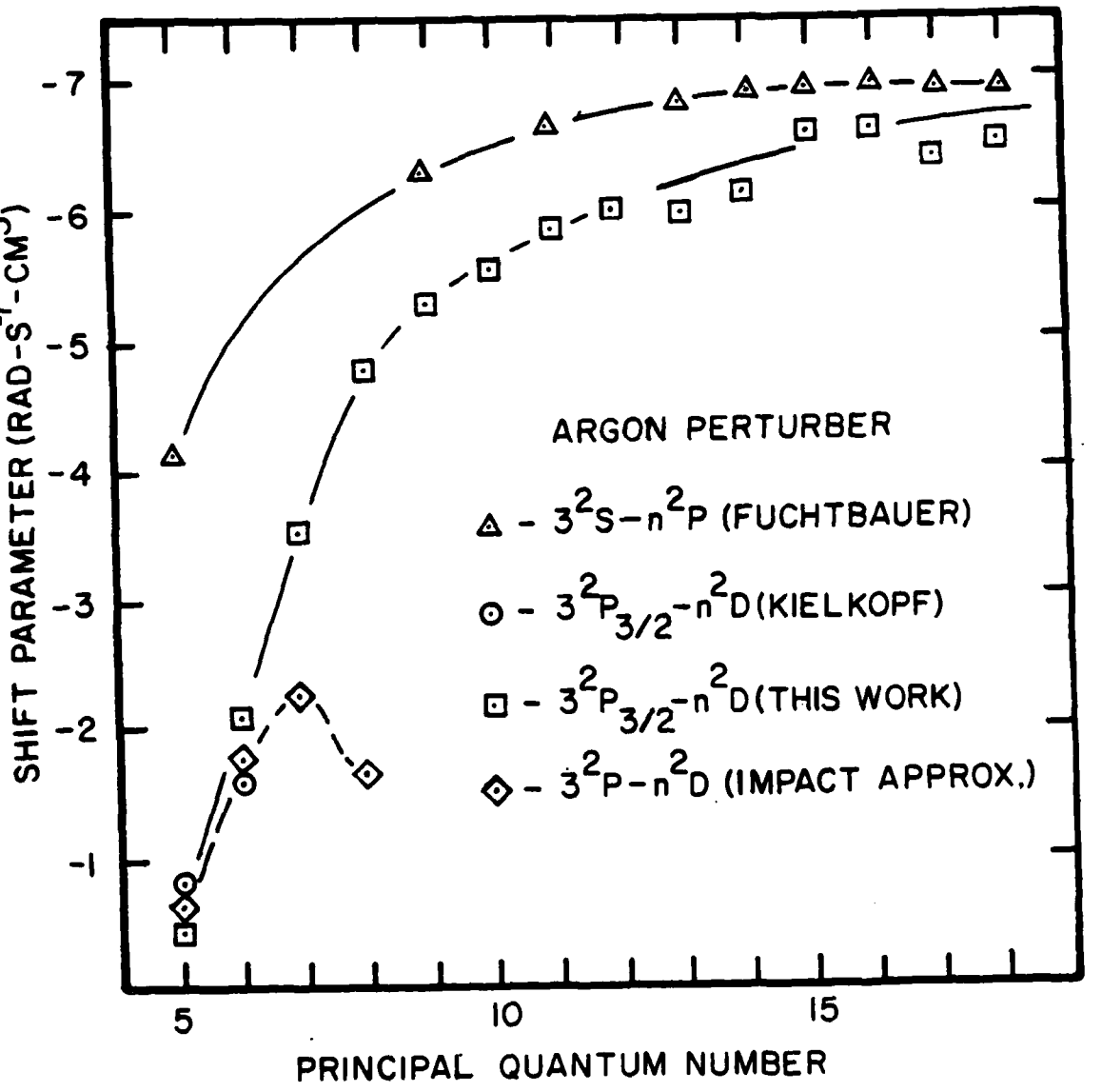

Figure 4. Spectral line shifts as a function of principal quantum number 3p - nd. Argon-Na at 400 Torr.

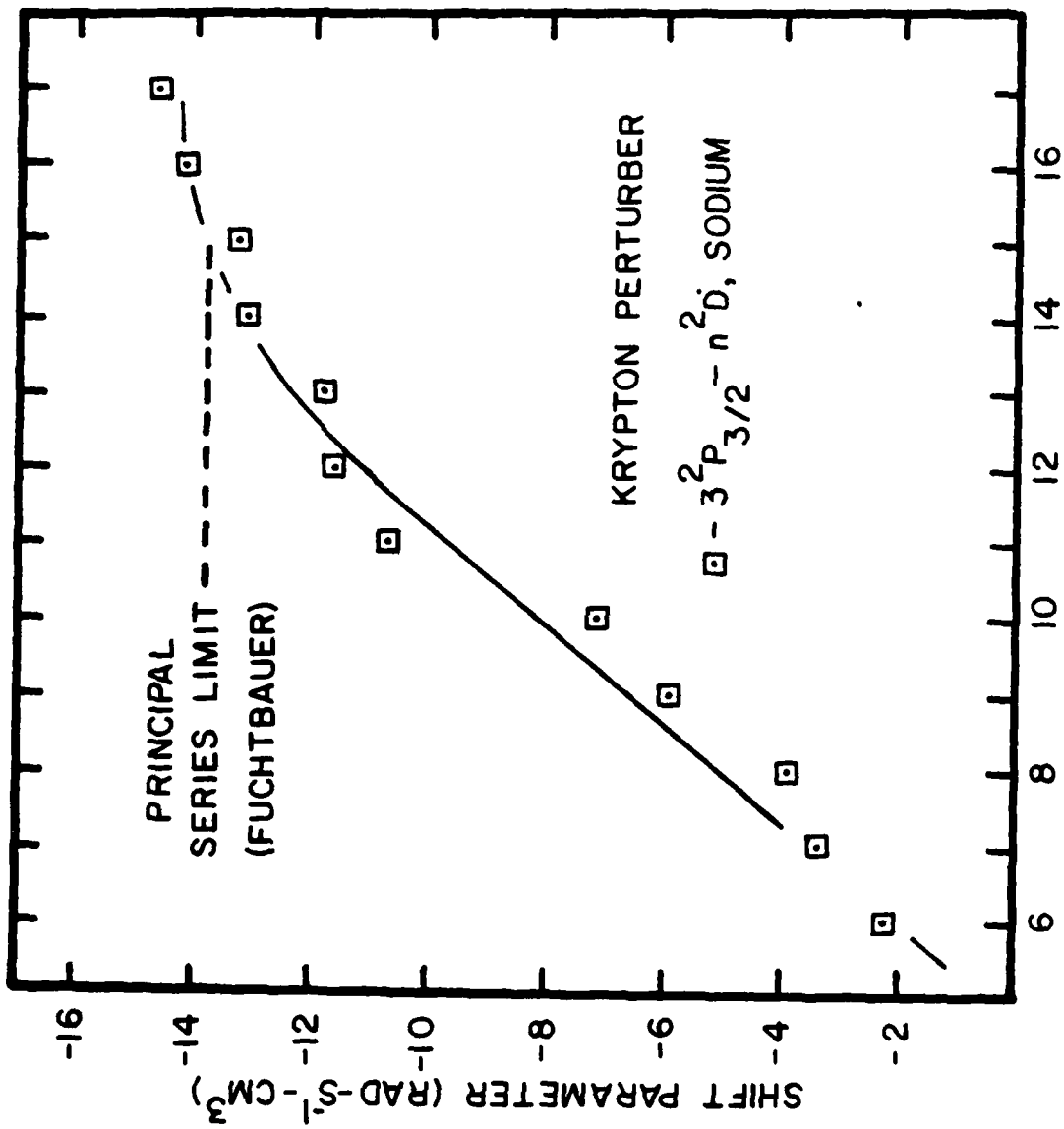

Figure 5. Spectral line shifts as a function of principal quantum number $3p - nd$. *Kr - Na at 400 Torr.*

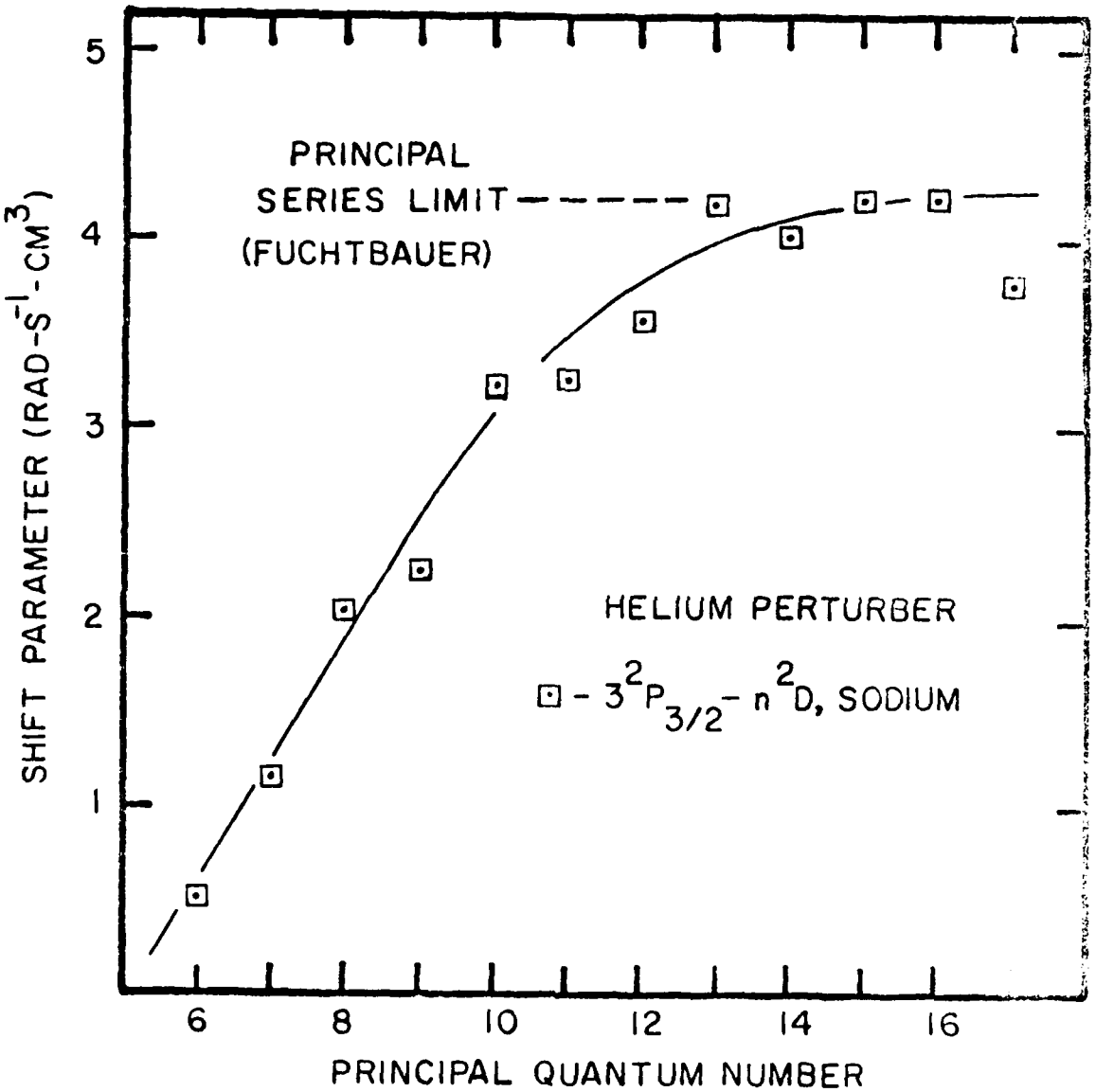

Figure 6. Spectral line shifts as a function of principal quantum number 3p - nd. He - Na at 400 Torr.

PHYSICAL REVIEW A VOLUME 26, NUMBER 3 SEPTEMBER 1982

Rare-gas, collision-induced shifts of the nD states of sodium

D. J. Krebs* and L. D. Schearer
Physics Department, University of Missouri-Rolla, Rolla, Missouri 65401
(Received 10 February 1982)

We have measured line shifts of the $3P$-nD transitions in sodium induced by collisions with helium, argon, and krypton for $n=5$ to 18. The shifts of the diffuse series transitions increase rapidly with principal quantum number and asymptotically approach the limit predicted by the Fermi model at high quantum numbers.

I. INTRODUCTION

The profile and frequency shift of atomic emission and absorption lines due to collisions have long been a source of information about the nature of low-energy collisions. Line profiles have been used to determine the short-range[1] and long-range[2] interaction potentials of radiator and perturber atoms while line shifts have been used to measure the cross section for collisions of low-energy electrons with perturber atoms.[3] Emission line shifts from plasmas have been used to measure electron density and temperature.[4]

The current interest in the collisional properties of Rydberg atoms has prompted new theoretical and experimental investigations of the line shapes and shifts of transitions to Rydberg levels. Brillet and Gallagher[5] have used Doppler-free two-photon spectroscopy to investigate the shift and broadening of the *ns* and *nd* Rydberg levels of Rb due to collisions with noble-gas atoms. The self-shift and self-broadening of alkali Rydberg levels has been investigated by Stoicheff and Weinberger[6] and Weber and Niemax[7] using Doppler-free two-photon techniques and a thermionic diode ionization detector. Mossberg *et al.*[8] have used a photon echo technique to determine the collisional dephasing rates of the Na *ns* and Na *nd* Rydberg levels which are related to the Lorentzian linewidths. A simple theory for the energy shifts of Rydberg levels was originally developed by Fermi.[9] Later refinements by Ivanov[10] and Alekseev and Sobelman[11] improved agreement with experimental data and included linewidth calculations. More recently, Omont[12] has developed formulas for line broadening at intermediate levels and broadening due to collisions with other alkali atoms.

We report here the measurement of line-shift parameters for the $3^2P_{3/2}$-$n\,^2D_{5/2,3/2}$ ($n\sim5$ to 17) transitions of sodium in collision with krypton, argon, and helium. The measurements for $n=5$ and 6 are in essential agreement with earlier measurements by Kielkopf and Knollenburg.[13] The measurements at high principal quantum number approach the same limit determined by Fuchtbauer *et al.*[14] for the principal-series transitions of Na.

II. APPARATUS

The basic experimental setup is illustrated in Fig. 1. Two N_2 pumped dye lasers provided 4-ns, 50-μJ pulses at two selected wavelengths. The first laser was tuned to the $3^2S\rightarrow3^2P_{3/2}$ transition in Na at 589 nm. The second laser beam was tunable across various $3^2P\rightarrow n\,^2D_{5/2,3/2}$ transitions at wavelengths between 500 and 408 nm, the threshold wavelength for direct excitation to the continuum from the 3^2P state.

The scanning laser output was delayed by 8 ns with respect to the fixed-frequency 589-nm laser and the two beams combined, using a beam-splitting mirror. The result was a superposition of

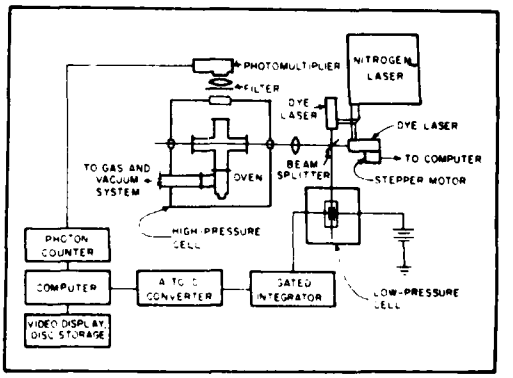

FIG. 1. Schematic representation of apparatus.

the two monochromatic beams to form two collinear dichromatic beams. One of the resulting dichromatic beams was directed to a cell containing sodium at ~370 °C and approximately 400 Torr of noble buffer gas. The other beam was directed to a cell containing sodium at ~200 °C with no buffer gas.

The high-pressure cell was a commercial stainless-steel cross fitted with sapphire windows on three sides. The sapphire windows were brazed to Kovar sleeves which were then welded onto Conflat flanges. A high-conductance bakeable valve connected the cell to a vacuum- and gas-handling system. The cell was baked for 24 h, at 400 °C, on a system with a base pressure of 5×10^{-7} Torr. A high-purity sodium ampoule was crushed in a cold finger and research-grade noble buffer gas was admitted to the desired pressure, typically ~0.5 atm. The low-pressure cell was a Pyrex cell with stainless-steel electrodes which contained sodium and no buffer gas. The low-pressure cell was operated at temperatures less than 250 °C to prevent darkening the cell by reaction of the sodium with the glass walls. The collinear laser pulses photoionize a small number of Na atoms in a three-photon process. The ion yield in the low-pressure reference cell was monitored directly by collecting the ions and electrons at appropriately biased parallel plates. The low-pressure cell was operated at a low temperature to keep the ion density below 10^8 cm^{-3}, thus avoiding space charge effects in the production region or at the collection plates which might influence charge collection efficiencies. The relative charge per pulse flowing through the load resistor was measured by integrating the voltage across the load resistor during a time window larger than the duration of the current pulse:

$$Q_{\text{pulse}} = \int_0^{t\gg\tau} I(t)dt = \frac{1}{R_L}\int_0^{t\gg\tau} V(t)dt\ , \quad (1)$$

where τ is equal to the signal pulse length. This was accomplished using a PAR 160 boxcar integrator in the fixed delay mode, which permitted an adjustable degree of signal averaging over several laser pulses. A 20-kΩ load resistor was generally used.

In the high-pressure cell, the small number of "seed" electrons produced by photoionization ultimately yielded a large ion-electron concentration. In this case, the seed electrons are superelastically heated by collisions with the highly populated $3p$ state. The hot electrons then collisionally ionize the Na. The details of the collisional processes occurring in this situation are given in Ref. 15. Measures and Cardinal provide a more general discussion.[16] In the late afterglow ($t > 2$ μs), ions and electrons recombine in a three-body process.

Recombination emission from the high-pressure cell was analyzed by an interference filter, detected by a photomultiplier, and recorded by an SSR 1110 synchronous photon counter. The photon counter counted recombination photons arriving at the detector within a time window extending from 1 to 500 μs after the firing of the lasers. Photon counts were accumulated for a fixed number of laser shots (typically 100 shots) after which time the accumulated total was reported to a microcomputer. The microcomputer saved the photon count data in memory along with the digitized output of the boxcar integrator and updated a video display of the data. It then advanced the wavelength drive of the scanning laser and enabled the photon counter, thus initiating another cycle. Signals from both cells were recorded simultaneously by the computer as the wavelength drive of the photoionizing laser was advanced across the transition.

III. OBSERVATIONS

Figure 2 illustrates the sequence of events occurring in the high-pressure cell after the arrival of the laser pulses. In the first ~4 ns, the resonant laser pulse populates the $3^2P_{3/2}$ level. The $3^2P_{1/2}$ level is rapidly populated due to collisions with the perturber atoms. The scanning laser pulse then populates the $n\,^2D$ level and also produces a small number of ions via photoionization of the $n\,^2D$ atoms. A strong initial fluorescence, due to associative excitation,[16] is followed by the rise and slow decay of emission resulting from excited states created in the

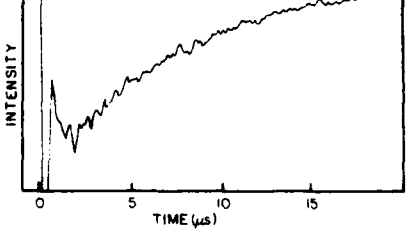

FIG. 2. Fluorescence intensity vs time after excitation for the $5d$-$3p$ transition. Early peak (off scale) is approximately 20 times more intense than the peak of the recombination fluorescence at $t = 2$ μs.

three-body electron stabilized recombination process.

In the experiment, the $3p$ level is first populated by the 4-ns pulse of photons from the fixed laser tuned to the $3s$-$3p$ resonance. Following an 8-ns delay, the scanning laser populates the nd state at a rate determined by the absorption cross section of the $3p$-nd transition. If one assumes that saturation effects associated with the scanning laser are weak or absent, it can be shown that the ultimate ion-to-electron density depends directly on the absorption cross section. The Appendix contains a detailed rate-equation analysis of the absorption-ionization processes involved in the experiment.

The fluorescence from atoms formed in the collisional-radiative recombination process is distinguished by the many-microsecond decay characteristic of the recombination rate. The details of the collisional-radiative model are discussed elsewhere.[17] The majority of atoms returning to the ground state do so via radiative decay from the $3p$ level. Similarly, the majority of atoms reaching the $3p$ level do so via a radiative decay from a low-lying nd or ns level. Consequently, the total recombination emission detected on a strong, low-lying transition represents a reasonable measure of the number of ions produced during the ionization process. Through the use of a similar argument, Hinnov showed that his measured intensities of the low-lying transitions of He and He^+ were related to the recombination coefficients of He^+ and He^{2+}, respectively.[18]

In principle, the $3p$-$3s$ recombination emission provides the best measure of the relative ion yield, but identical results were obtained monitoring the $4d$-$3p$ or $5d$-$3p$ fluorescence. Experimentally, it was advantageous to use the $5d$-$3p$ transition, and the data presented in this paper were all taken in this manner. Because of the long, slow decay of the recombination fluorescence, photon counting techniques were used to detect the recombination emission.

The recombination emission as a function of scanning laser intensity was measured for a number of transitions with the laser wavelength fixed at line center. The ionizing laser intensity was varied from about 0.05 to 10 kW through the use of an attenuating filter composed of crossed polaroids. The angle between the polarization axes of the crossed polaroids was slowly scanned with a motor drive and the transmission of the filter was monitored through the use of a white light source and a 0.1-m monochromator. The setting of the monochromator was adjusted to be the same as that of the laser so that the attenuation of the filter at the laser wavelength was measured. The output of the monochromator was detected with a photomultiplier tube and the resulting signal was digitized and read by the computer. When an incremental change in the transmission of the filter was determined, the computer read the number of recombination photons recorded at that attenuation and the number of laser shots over which those photons were counted. The integrated recombination fluorescence versus laser intensity was output in real time to an oscilloscope display and the data was stored on magnetic disk at the end of each run.

Figure 3 shows the intensity dependence of the two-step photoionization process for two transitions. Figure 4 shows a theoretical curve generated through the use of the theoretical analysis of the Appendix. The $6d$-$3p$ transition exhibits the greatest level of saturation, but even this curve exhibits quadratic dependence at small intensities, indicating that two laser photons are involved in the initial absorption.

Figure 5 is a scan of the relative ion yield, from the integrated $5d \rightarrow 3p$ fluorescence, versus laser wavelength showing the various nl-$3p$ transitions. The merger of the transition series near the ionization threshold at 408 nm is apparent. Figure 6 is a simultaneous scan of the relative ion yield in the high-pressure cell and the low-pressure cell taken for the $8d \rightarrow 3p$ transitions. The scan is a doublet in the high-pressure cell due to collisional mixing of

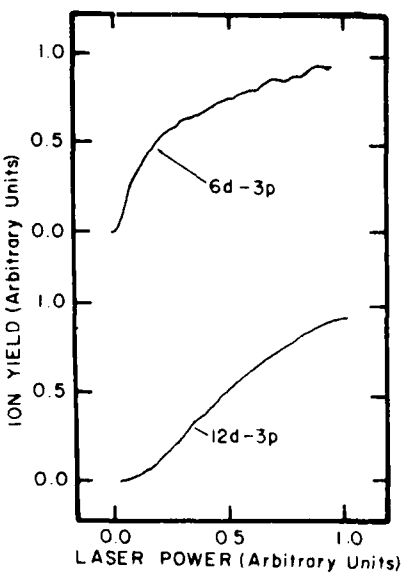

FIG. 3. Integrated fluorescence vs intensity of the second laser which was tuned to the $6d$-$3p$ transition.

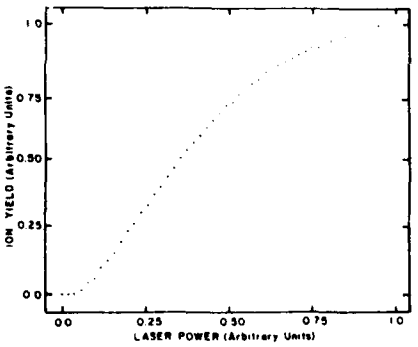

FIG. 4. Plot of Eq. (A4) for $R_2=4R_1$: Ion yield vs laser intensity. At low intensities the ion yield depends quadratically on the laser intensity indicating that a two-photon process is involved. At the maximum intensity saturation effects occur.

the $3^2P_{3/2,1/2}$ levels by buffer-gas atoms. For the data shown the buffer-gas pressure is 400 Torr and the scanning laser power is approximately 2 kW.

Through the use of the detailed analysis in the Appendix, the experimental wavelength dependence of the ion yield can, in principle, be deconvoluted to obtain the line profile of the $3p$-nd transitions. Because the linewidth parameters for these transitions have recently been measured using a photon echo technique,[8] it was decided to concentrate on the line shifts, which cannot be measured by photon echo techniques. Because the ionization yield is a monotonically increasing function of the $3p$-nd absorption cross section, the wavelength of maximum ionization corresponds to the maximum of the lineshape function. The hyperfine splitting of the $n^2D_{5/2,3/2}$ and 3^2P levels is much smaller than the measured shifts. Hence, any shift in the line maximum due to the broadening of the unresolved structure is small and the maximum of the lineshape function defines the line center. Thus, taking scans similar to that of Fig. 6, it was possible to measure the line shifts without resorting to a detailed deconvolution of the resonance ionization spectra.

IV. RESULTS AND DISCUSSION

The theory of collisional line broadening and shifts has been reviewed by several authors. A fairly general method has been developed by Anderson[19] which provides a way of predicting line profiles and shifts from the interatomic molecular potentials of the radiator and perturber atoms. With appropriate simplifying assumptions, Anderson theory reduces to the less general impact theory. Impact theory is applicable provided the time between perturbing collisions is much greater than the duration of those collisions. Departure from impact conditions occurs in either of two ways: (1) with high perturber densities or (2) with highly excited radiator atoms for which the cross section for

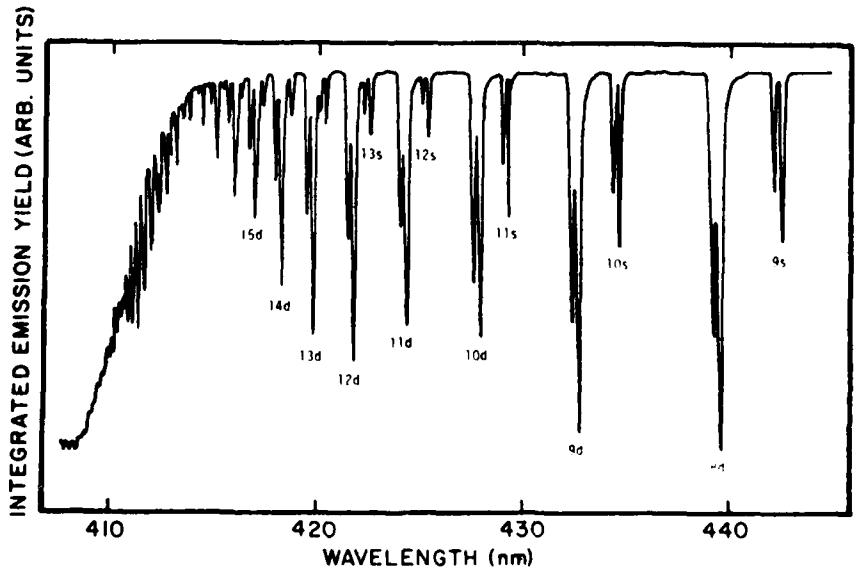

FIG. 5. Ion yield vs wavelength of the second laser. At 408 nm, photoionization out of the $3p$ level occurs directly. At the longer wavelengths, photoionization occurs via a resonant intermediate level (nd or ns).

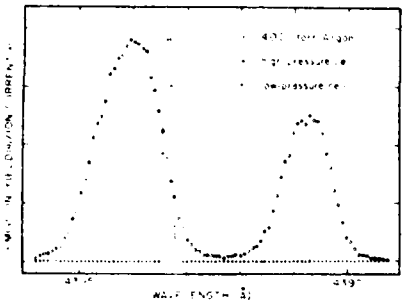

FIG. 6. Ion yield vs wavelength as the second laser is tuned through the $8d$-$3p$ transition. Open circles are from the high-pressure cell. Two lines shown represent excitation of both the $3P_{3/2}$ and $3P_{1/2}$ levels which are collisionally mixed. Solid line is obtained from the low-pressure cell and only a single peak appears.

the collision between the radiator and perturber atoms is large.

Royer[20] has successfully applied Anderson theory to the high-pressure regime of the first condition. The theories applicable in the second case have been developed by Fermi,[9] Ivanov,[10] Alekseev and Sobelman,[11] and Omont.[12] The data presented in this section illustrate the variation of the line-shift parameters with energy level for levels extending from those for which impact theory is applicable through an intermediate regime, and into the Rydberg regime.

Fermi's theory predicts that the shift of the energy levels of excited Rydberg atoms Δ due to collisions with perturber atoms approaches an asymptotic limit given (in atomic units) by

$$\Delta = 2\pi LN - 10\alpha N^{4/3} , \tag{2}$$

where Δ is equal to the shift, α is equal to the dipole polarizability of the perturber atoms, N is equal to the density of perturber atoms, and L is equal to the zero-energy-electron scattering length of the perturber atom. This result is independent of the properties of the radiator atom or the angular momentum state of the Rydberg level. The first term in Fermi's equation, called the scattering term, accounts for the scattering of the Rydberg electron by the noble-gas atoms. The second term accounts for the change in energy of the system due to the polarization of perturber atoms which lie within the orbit of the Rydberg electron and are therefore subject to the field of the unshielded core.

Ivanov[10] has proposed that a more exact expression for the scattering term component of the line shift Δ_{sc} is given by

$$\Delta_{sc} = 2\pi \left| L + \frac{4}{3}\frac{L\alpha}{n^2} \ln\left| \frac{e}{n} \right| + \frac{\bar{\gamma}}{n^2} \right| N , \tag{3}$$

where n is equal to the effective principal quantum number, e is equal to 2.718, and $\bar{\gamma}$ is equal to a constant characteristic of the perturbing atom. For the conditions of this experiment Ivanov's expression is no more than a 10% correction to the scattering term given by Fermi.

Alekseev and Sobelman[11] have shown that provided

$$\frac{2\alpha}{v} N \ll 1 , \tag{4}$$

where v = the average velocity of the perturber atom, the polarization term Δ_p is given by

$$\Delta_p = -6.22(\alpha^2 v)^{1/3} N . \tag{5}$$

Fermi's formula was shown to be appropriate for cases in which

$$\frac{2\alpha N}{v} \gg 1 . \tag{6}$$

For the conditions of this experiment $2\alpha N/v \sim 0.06$, and therefore the formula derived by Alekseev and Sobelman is used.[11]

Thus, theory predicts a shift of

$$\Delta = \Delta_{sc} + \Delta_p = 2\pi \left[L + \frac{4}{3}\frac{L\alpha}{n^2} \ln\left[\frac{e}{n} \right] + \frac{\bar{\gamma}}{n} \right] - 6.22(\alpha^2 v)^{1/3} N . \tag{7}$$

Figures 7, 8, and 9 show the measured line-shift parameters for the $3^2P_{3/2}$-$n\,^2D$ transitions of sodium due to collision with argon, krypton, and helium perturbers, respectively. The temperature of the cell was ~ 600 K. Also shown are the results obtained by Fuchthauer and Schultz[15] for the principal-series transitions and the theoretical predictions of Eq. (7). The agreement with theory is quite good at the highest quantum numbers, except for the argon data which is about 10% below the theoretical predictions. Brillet and Gallagher[5] have also reported unexpectedly small shifts for the $19d$ level of Rb perturbed by argon. A breakdown of the scattering length approximation for the Rydberg nd levels perturbed by argon was predicted by Omont[12] in the calculation of mixing cross sections, and perhaps this breakdown is reflected in the data presented here. The agreement at high quantum number with the shifts found by Brillet and Gallagher[5] for the Rydberg ns levels of Rb is good. At

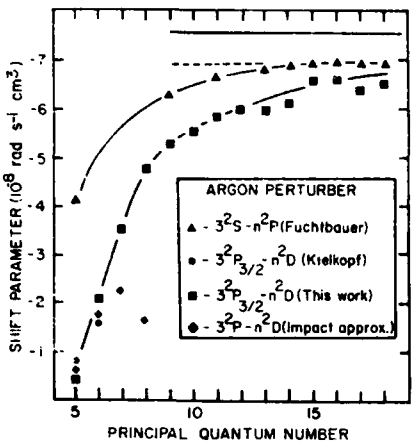

FIG. 7. Line-shift parameters for the *nd* states of Na due to collisions with argon at 400 Torr and cell temperature of 600 K. Solid line shown is the asymptotic limit obtained from Eq. (7).

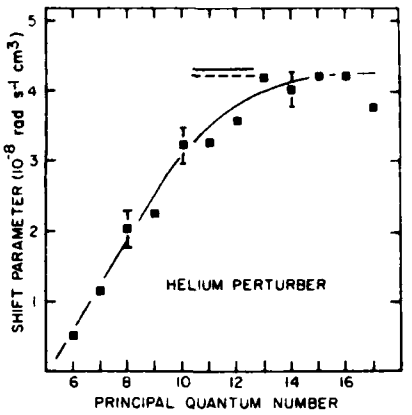

FIG. 9. Line-shift parameters for the *nd* states of Na due to collisions with He at 400 Torr. Solid line is the limit obtained from Eq. (7). Dashed line is the limit obtained by Fuchtbauer *et al.* (Ref. 14) for the $3s$-np series.

the highest energy levels, the shifts are seen to approach the same asymptotic limit as measured by Fuchtbauer for the principal-series transitions. This is the behavior expected based on Fermi's analysis. One notes that the shift for helium is positive corresponding to a blue shift while the data for argon and krypton is negative corresponding to a red shift. These shifts are correlated with the sign of the perturbing atom's electron scattering length.

In the case of argon, the previous experimental results of Kielkopf and Knollenburg[13] at the lowest energy levels are shown along with the predictions of binary-collision approximation calculations. The impact-theory calculations are extensions of the theoretical work of Kielkopf and Knollenburg to higher energy levels. It is seen that, for argon, the impact approximation departs sharply from experiments for levels above about $n=6$. This is to be expected since the impact approximation assumes that the time between collisions is much greater than the duration of collisions. At $n=7$, in argon, the time between collisions τ is (in sec)

$$\tau \simeq \frac{1}{N\sigma\langle V\rangle} \sim 10^{-11},$$

while the collision duration is about 10^{-12} sec.

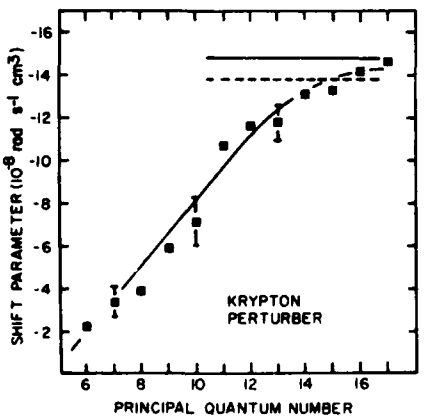

FIG. 8. Line-shift parameters for the *nd* states of Na due to collisions with krypton at 400 Torr. Solid line is the asymptotic limit obtained from Eq. (7). Dashed line is the limit obtained by Fuchtbauer *et al.* (Ref. 14) for the $3s$-nP series.

CONCLUSIONS

The utility of resonance ionization techniques for studying excited-excited transition line shifts has been demonstrated. The dependence of the integrated recombination signal on laser intensity is consistent with the model of stepwise ionization followed by electron-impact ionization of excited atoms followed by collisional radiative recombination.

The diffuse series ($3^2P_{3/2}$-$n\,^2D_{5/2,3/2}$) transitions of sodium exhibit less energy shift at low principal quantum number than do the principal-series ($3^2S_{1/2}$-$n\,^2P_{3/2,1/2}$) transitions. The shifts of the diffuse series transitions increase rapidly with principal quantum number and asymptotically approach the same limit as previously measured for the principal-series transitions. The equivalence of the two limits at high quantum number is the

behavior expected based on theory. The agreement of the data with scattering-length theory is excellent, except for the argon shifts, which are about 10% smaller than predicted. A dramatic departure of the measured shifts from the impact-approximation predictions occurs at levels for which the binary-collision conditions no longer apply.

ACKNOWLEDGMENT

This work was supported by the Office of Naval Research.

APPENDIX

In order to simplify the analysis, the experiment was conducted with the arrival of the scanning laser pulses in the reaction region optically delayed by about 8 ns with respect to the arrival of the resonant laser pulses. When the scanning laser pulses reached the reaction region, the $3p$ atoms were decaying with their trapped lifetime of about 250 ns, so that during the 4 ns scanning laser pulse, radiative decay terms may be neglected in a rate equation analysis. Because the collisional dephasing rate due to collisions with buffer atoms is such that the excited atom loses phase memory before further absorption or emission may occur, coherence effects may be neglected and a rate equation analysis is appropriate.[21]

We, thus, write rate equations describing the resonance ionization process occurring during the scanning laser pulse

$$\frac{dN_{3p}}{dt}=\Gamma_{21}(\nu)IN_{nd}-\Gamma_{12}(\nu)IN_{3p}\ ,$$

$$\frac{dN_{nd}}{dt}=-\Gamma_{21}(\nu)IN_{nd}+\Gamma_{12}(\nu)IN_{3p}-\sigma_I IN_{nd}\ ,$$

$$\frac{dN^+}{dt}=\sigma_I IN_{nd}\ , \tag{A1}$$

where $\Gamma_{21}(\nu)$ is the cross section for induced emission from the Na nd level, $\Gamma_{12}(\nu)$ is the cross section for absorption from the Na $3p$ level, σ_I is the photoionization cross section of Na nd atoms, I is the intensity of the scanning laser, ν is the laser frequency, N_{nd} is the population density of the excited nl level, and N_{3p} is the population density of the $3p$ level.

We have used the fact that the laser bandwidth is much narrower than the transition bandwidth. The transition strength contains the line-shape function

$$\Gamma_{ij}(\nu)=B_{ij}K(\nu)\ , \tag{A2}$$

where $K(\nu)$ is the normalized line-shape function and B_{ij} is the Einstein "B" coefficient. We have neglected terms involving spontaneous decay and recombination because those processes are negligible within the 4-ns time range of the atom-field interaction. For the time dependence of the laser pulse, we assume a square-wave form

$$I(t)=I[\theta(t)-\theta(t-\tau)]\ , \tag{A3}$$

where $\theta(t)=1$ if $t>0$, and 0 if $t<0$, and τ is the laser pulse width.

The rate equations are then solved to give the net ionization produced by a square-wave laser pulse

$$N^+(\tau)=\int_0^\tau \frac{dN^+}{dt}dt\ , \tag{A4}$$

$$N^+(\tau)=n_e(\tau)=N_{3p}(0)\left[1-e^{-R_1 I\tau}\left\{\frac{R_1}{R_2}\sinh(R_1 I\tau)+\cosh(R_2 I\tau\right\}\right]\ ,$$

where $R_1=(\Gamma_{21}+\Gamma_{12}+\sigma_I)/2$, $R_2=(R_1^2-\Gamma_{12}\sigma_I)^{1/2}$, and $N_{3p}(0)$ is the density at $t=0$.

Equation (A5) describes the intensity and line-shape dependence of the ionization resulting from the two-step photoionization of the Na $3p$ atoms which occurs during the 4-ns [full width at half maximum (FWHM)] laser pulse. At low intensity, Eq. (A4) reduces to $N^+=(\sigma_I I\tau)(\Gamma_{12}I\tau)$, or simply the product of two absorption probabilities. The electrons created in this process are heated via superelastic collisions with the large density of excited $3p$ atoms. The superelastic collision time for these electrons is about 1 ns.[22] Additional ionization may result from electron-impact ionization of the Na $3p$ and Na nd atoms by the superelastically heated electrons. Typical cross sections[23] for these collisions are $\sigma\sim10^{-15}$ cm^2 so that the rate for collisional ionization by an initial population density of 10^{12} cm^{-3} is about 10^5 s^{-1}. This is small compared to the radiative decay rates of these states so that we may neglect ionization loss in writing the rate equations for the excited-state populations.

For the population densities of the various levels following the decay of the laser pulses, one writes

$$\frac{dN_{3p}}{dt} = -A_{3p}N_{3p} ,$$
$$\frac{dN_{nl}}{dt} = -A_{nl}N_{nl} , \tag{A5}$$
$$\frac{dN^+}{dt} = (K_{1c}N_{3p} + K_{2c}N_{nl})n_e ,$$

where A_{nl} is the spontaneous radiative decay rate of the nl level and K_{1c} and K_{2c} are electron impact ionization rates of the $3p$ and nl levels, respectively. Recombination is negligible while the N_{3p} population is significant.

The Na nl concentration at the end of the laser pulse, $N_{nl}(\tau)$, is given by the solution of Eqs. (A1) and (A4):

$$N_{nl}(\tau) = \frac{\Gamma_{12}N_{3p}(0)}{R_2}\exp(-R_1 I\tau)\sinh(R_2 I\tau) . \tag{A6}$$

Integrating Eqs. (A5) from $t=\tau$ to ∞, one sees that the ultimate electron density (ignoring diffusion and recombination losses) is

$$n_e = n_e(\tau)\exp\left\{N_{3p}(0)\left[\frac{K_{1c}}{A_{3p}} + \frac{K_{2c}}{A_{nl}}\left[\frac{\Gamma_{12}}{R_2}e^{-R_1 I\tau}\sinh(R_2 I\tau)\right]\right]\right\} , \tag{A7}$$

where $n_e(\tau)$ is given by Eq. (A4).

Equation (A7) shows that the ultimate electron concentration is given by the photoionization yield $n_e(\tau)$ multiplied by an exponential factor which accounts for electron-impact ionization of excited atoms. This exponential factor depends on the initial Na $3p$ concentration, the electron-impact ionization rates, the radiative lifetimes of the excited states, and the degree of excitation of the $3p$-nd transition.

The exponential factor is independent of laser intensity whenever

$$\frac{K_{1c}}{A_{3p}} \gg \frac{K_{2c}}{A_{nl}}\left[\frac{\Gamma_{12}}{R_2}e^{-R_1 I\tau}\sinh(R_2 I\tau)\right] , \tag{A8}$$

which for an unsaturated transition ($\Gamma_{12}I\tau \ll 1$) reduces to the condition

$$\frac{K_{1c}}{A_{3p}} \gg \frac{K_{2c}}{A_{nl}}(\Gamma_{12}I\tau) . \tag{A9}$$

Provided these conditions are satisfied, the dependence of the ultimate electron density on the power and wavelength of the scanning laser is the same as that of the initial electron density produced by the laser pulses. A prediction of the intensity dependence of Eq. (A7) requires a detailed knowledge of the electron-impact ionization rates which depend on electron temperature during the ionization process. The shape of the dependence of initial ion yield on laser intensity, however, depends only on the relative magnitudes of R_1 and R_2 which, in turn, depend on the relative magnitudes of Γ_{12} and σ_I. The discussion of the preceding paragraph shows that it may be reasonable to expect this dependence to be replicated in the final ion production. Approximate calculations of Γ_{12} and σ_I show that the photoionization step and resonant absorption step should be of comparable magnitudes and approaching saturation.

Following the ionization process, collisional-radiative recombination proceeds on a many-microsecond time scale,[15] with the ions and electrons recombining into excited levels of the neutral atom. Those excited atoms may then radiatively decay, be collisionally reionized, or be collisionally excited-deexcited.

*Present address: McDonnell-Douglas Astronautics Co., St. Louis, Missouri.

[1]R. E. M. Hedges, D. L. Drummond, and Alan Gallagher, Phys. Rev. A 6, 1519 (1972).
[2]B. Cheron, R. Scheps, and A. Gallagher, Phys. Rev. A 15, 651 (1977).
[3]H. Margenau and W. W. Watson, Rev. Mod. Phys. 8, 22 (1936).
[4]H. R. Griem, *Plasma Spectroscopy* (McGraw-Hill, New York, 1964).
[5]Wan-Ü L. Brillet and A. Gallagher, Phys. Rev. A 22, 1012 (1980).
[6]B. P. Stoicheff and E. Weinberger, Phys. Rev. Lett. 44, 733 (1980).

[7]K. H. Weber and K. Niemax, Opt. Commun. 28, 317 (1979); 31, 52 (1979).
[8]A. Flusberg, R. Kachru, T. Mossberg, and S. R. Hartman, Phys. Rev. A 19, 1607 (1979); R. Kachru, T. W. Mossberg, and S. R. Hartman, *ibid.* 21, (1980).
[9]E. Fermi, Nuovo Cim. 11, 157 (1934).
[10]G. K. Ivanov, Opt. Spektrosk. 40, 965 (1976) [Opt. Spectrosc. 40, 554 (1976)].
[11]V. A. Alekseev and I. I. Sobelman, Zh. Eksp. Theor. Fiz. 49, 1274 (1965) [Sov. Phys.—JETP 22, 882 (1966)].
[12]A. Omont, J. Phys. (Paris) 38, 1343 (1977).
[13]J. F. Kielkopf and R. B. Knollenburg, Phys. Rev. A 12, 559 (1975).
[14]C. Fuchtbauer, P. Schulz, and A. F. Brant, Z. Phys. 90, 403 (1935).
[15]D. J. Krebs and L. D. Schearer, J. Chem. Phys. 75, 3340 (1981).
[16]R. M. Measures and P. T. Cardinal, Phys. Rev. A 23, 804 (1981).
[17]D. R. Bates, A. E. Kingston, and R. W. P. McWhirter, Proc. R. Soc. London 267, 297 (1962).
[18]E. Hinnov, Phys. Rev. 147, 197 (1966).
[19]P. W. Anderson and J. O. Tallman, *Conference on the Broadening of Spectral Lines* (University of Pittsburgh Press, Pittsburgh, 1955).
[20]A. Royer, Phys. Rev. A 22, 1625 (1980).
[21]G. S. Hurst, M. G. Payne, S. D. Kramer, and J. P. Young, Rev. Mod. Phys. 51, 767 (1979).
[22]R. M. Measures, J. Appl. Phys. 48, 2673 (1977).
[23]H. S. W. Massey, E. H. S. Burhop, and H. B. Gilbody, *Electronic and Ionic Impact Phenomena* (Oxford University Press, Oxford, 1969), Vol. 1.

Electron density measurements in a laser induced Na plasma[a)]

D. J. Krebs[b)] and L. D. Schearer

University of Missouri-Rolla, Physics Department, Rolla, Missouri 65401
(Received 13 November 1981; accepted 9 December 1981)

The optical emission spectrum of a recombining Na plasma is observed. The shift and broadening of the spectral line emission due to electron collisions is observed. Electron densities on the order of 5×10^{14} cm^{-3} are calculated from the shift measurements. The results agree well with electron densities obtained in the same system from Saha plots of excited state densities.

I. INTRODUCTION

The electron density in a partially ionized plasma is an important parameter in determining the properties of the gaseous discharge. The current interest in discharge switches, high-power pulsed laser discharges, recombination lasers, and laser induced plasmas has made the determination of the electron density in pulsed systems a necessity.

A variety of techniques exist for the determination of the electron density in a decaying plasma; however, spectral measurements have the advantage that noncontact observations can be made and small volumes sampled within small time intervals.

In this article we report the observation of spectral line shifts and broadening due to electron collisions in a recombining Na plasma. From measurements of the spectral line shifts, the electron density is calculated. The electron density thus obtained is compared with measurements inferred from Saha–Boltzmann plots of the excited Na states in local thermodynamic equilibrium with the electrons. These electron density measurements are also compared with charge removed from the plasma by an applied electric field. The plasma for the experiment described here consists of a line charge of approximately 0.5 mm diameter with electron densities up to 10^{15} cm^{-3} in a cell containing Na (~ 1 Torr) and argon (400 Torr).

II. EXPERIMENTAL APPARATUS

The sodium atoms along with a rare-gas buffer are contained in a stainless steel cross with sapphire windows. The structure is placed in an oven enabling temperatures up to 700 K to be obtained. The Na plasma is produced by laser excitation in a 2 or 3 photon absorption process via the Na($3p$) state. The buffer gas, typically argon at several hundred Torr, is used to eliminate diffusion losses of ions, electrons, and excited atoms from the observation region during the course of the experiment.

Two tunable dye lasers pumped by a single N_2 laser provided 4 ns, 50 μJ pulses at two different frequencies. One laser is tuned to excite one of the $3\,^2P$ sodium levels at 589 nm while the second laser can be tuned to wavelengths between 406 and 564 nm. At 406 nm, the photons have just sufficient energy to photoionize the $3p$ atom. The bandwidth of the lasers is approximately 0.4 Å (FWHM). The two laser beams are passed collinearly through the Na cell and focused at the cell center to ~ 0.3 mm diameter spots. The beam divergences were sufficiently small over the observation region that a very nearly cylindrical column of excited vapor is created. The fluorescence at 90° to the axis of the excited region is observed by an S-20 photomultiplier coupled to a 0.5 m Jarrell–Ash monochromator. The photomultiplier output is analyzed by a PAR 160 boxcar integrator, an SSR 1110 synchronous photon counter, or a Tek 5441 storage oscilloscope with a fast sampling head. A schematic representation of the apparatus is shown in Fig. 1.

III. EXPERIMENTAL OBSERVATIONS

A. Two photon processes

If the second laser is tuned to 406 nm, a sodium atom can be ionized in a two photon, resonant absorption process via the $3p$ state. The laser intensities and pulse widths (50 μJ, 4 ns) do not produce more than a relatively small number (~ 10^{12} cm^{-3}) of "seed" electrons via the photoionization process. However, collisional mechanisms involving densely populated excited states and the seed electrons can lead to nearly complete ionization of the Na vapor. This ionization mechanism has been discussed by Lucatorto and McIlrath[1] and Measures and Cardinal,[2] while energy pooling processes leading to excited state populations in the early afterglow have been discussed by Bearman and Levanthal[3] and Allegrini *et al.*[4] We have examined the kinetics of the energy pooling process and measured rate constants for the formation of the $4d$, $5d$, $6d$, and $6s$ states by collisions between two Na($3p$) atoms.[5]

Optical emission from $nd-3p$ transitions in Na in the afterglow of the laser pulses under the conditions described above is observed. The individual transitions are isolated with a monochromator. A PAR Boxcar Integrator with an aperture of 20 ns is used to temporally scan the wavelength isolated line. Figure 2 shows the fluorescence intensity versus time in the afterglow of the laser pulse for the $5d-3p$ transition. The optical pulse consists of two components: A strong initial pulse of approximately 100 ns duration followed by a rise and slow decay of the fluorescence. The early, fast component is associated with excited state populations pro-

a)Work supported by the Office of Naval Research.
b)Present address: McDonnell Douglas Co., St. Louis, MO 63166.

 0021-9606/82/062925-06$02.10

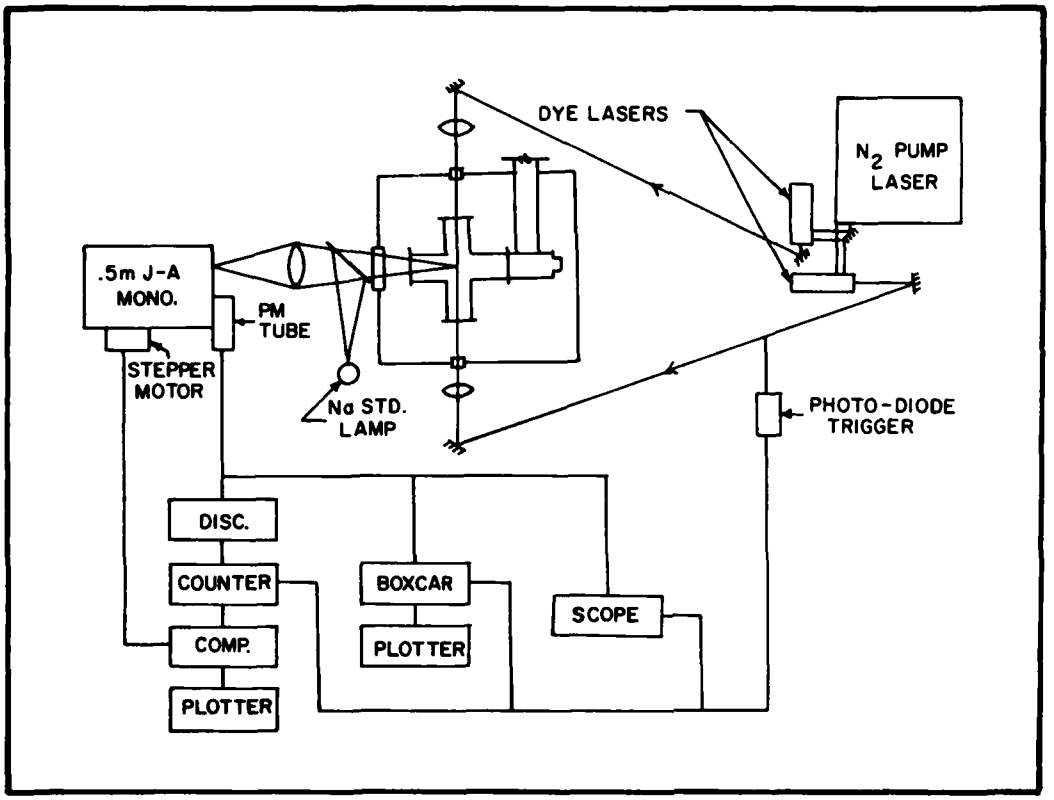

FIG. 1. Schematic of the apparatus.

duced by collisions of two $3p$ atoms. States which are energetically accessible to a Boltzmann distribution of the $3p$ atoms are populated within this first 100 ns following the 589 nm laser pulse. Subsequent to the decay of this fast component a slow component appears and decays on a many microsecond time scale. Emission in this slow component is due to three-body, electron stabilized recombination.

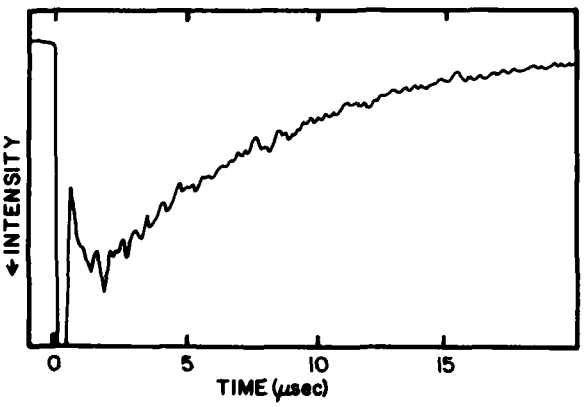

FIG. 2. Fluorescence intensity vs time after laser excitation for the $5d \rightarrow 3p$ transition with both lasers employed. The early fluorescence peak, which is off-scale, is approximately 20 times more intense than the peak of the recombination fluorescence at $t = 2\ \mu s$. The second laser is tuned to the ionization threshold of the $3p$ state at 408 nm.

B. Recombination fluorescence

The fluorescence appearing 2 μs after the laser pulses is due to the recombination process. With the Boxcar Integrator set to a delay of 2 and 0.5 μs aperture a

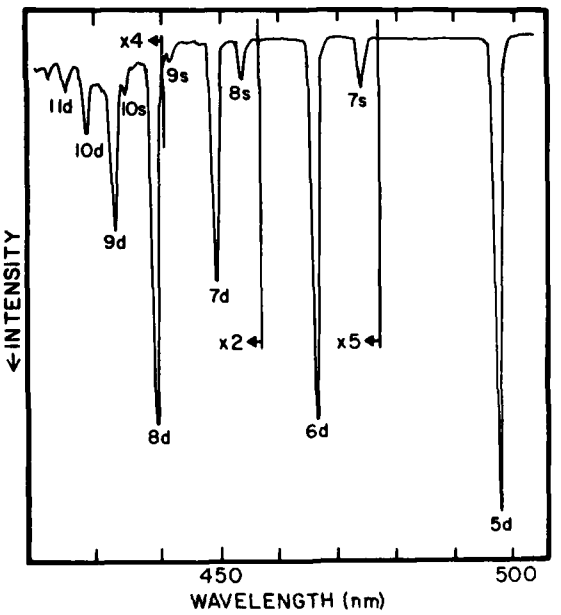

FIG. 3. Recombination fluorescence at $t = 2\ \mu s$ vs wavelength. Scan resolution is 0.8 nm (FWHM). The second laser is fixed at 408 nm.

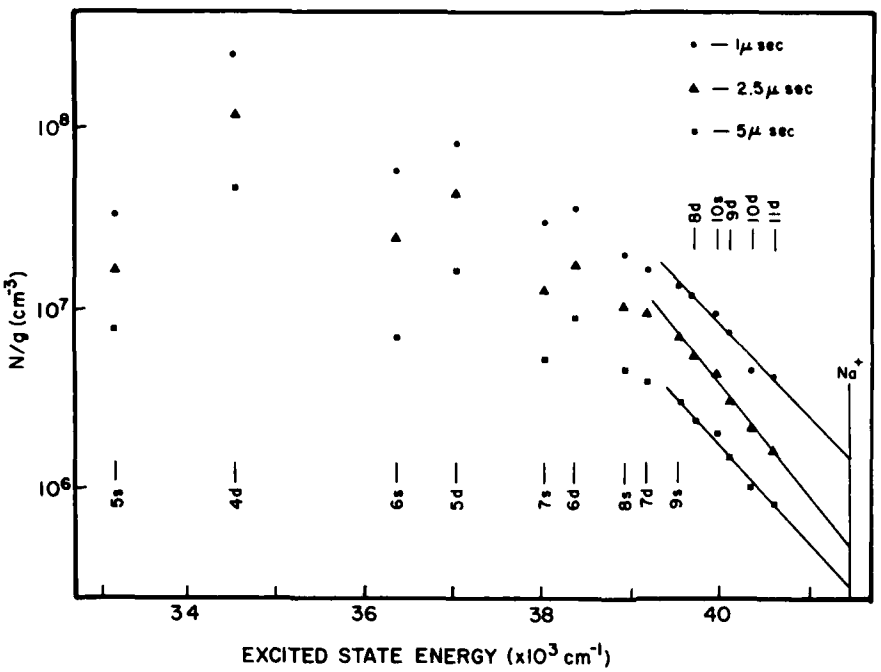

FIG. 4. Saha–Boltzmann plot of excited state densities vs energy level.

monochromator scan of the emission produces the spectrum shown in Fig. 3. The monochromator detection system is calibrated against an absolute standard lamp; thus absolute intensity measurements of the transitions along with radiative decay rates yield absolute excited state densities. Figure 4 is a plot of the absolute excited state density versus the excited state energy. Levels within 0.25 eV of the ionization limit appear to be in local thermodynamic equilibrium with the electrons. Applying the Saha equation

$$n_e^2/N^* = (2g_{\rm ion}/g^*)(2\pi mkT_e)^{3/2}\exp[-(E_{\rm ion}-E^*)/kT_e]\,, \quad (1)$$

one obtains the electron temperature T_e and the electron density n_e. The electron temperature depends only on relative intensities, while the electron density depends on an absolute calibration of the detection system. For the data shown in Fig. 4, we obtain $T_e = 900$ K and $n_e = 3.4\times10^{14}$ cm^{-3}, 2.5 μs after the laser pulse. The density measurements are believed accurate within a factor of 3; the electron temperature is accurate to within 10%.

C. Line shift discussion and results

Shifts in the energies of the spectral lines emitted by the Na plasma occur as a result of collisions of the excited Na atoms with both the heavy particles (noble-gas buffer atoms) and/or the plasma electrons. If the collisional events leading to the excited state populations occur in the early afterglow where the electron density is small, any emission line shifts must be associated with collisions of the excited state with the large density of rare-gas buffer atoms. If, on the other hand, the fluorescence from excited states is observed late in the afterglow where the electron density is large, the emission lines are broadened by both collisions with the buffer gas atoms and the large density of electrons. The line shifts due to electron collisions are rather extensively described by Griem,[7] while Kielkopf and Knollenburg[6] discuss line shifts of the Na 5*d*, 6*d*, and 7*d* levels, due to collisions with argon atoms. In order to determine the shifts associated with electron collisions it is necessary to separate out the effects due to the buffer gas. At first glance, it would appear that the perturbations due to the buffer gas could be isolated by measuring the shifts as a function of pressure and extrapolating to zero pressure. However, the role of the buffer gas is to confine the excited state populations and ion/electrons to the region defined by the laser beam. At buffer gas densities above approximately 400 Torr the major loss of electron/ion density is via collisional-radiative recombination. At buffer gas densities less than this, a reduction of the electron density by ambipolar diffusion becomes increasingly important. Consequently, varying the buffer gas pressure also changes the electron loss rate. We are thus forced to devise an alternate technique.

1. Pressure shifts: Three photon absorption processes

In Sec. III B, the optical emission from the ionized volume at times greater than 0.5 μs after the laser pulse was described in terms of collisional-radiative recombination processes. The excited, bound states have lifetimes considerably shorter than the microsecond time scale of Fig. 2. The excited states are either quenched radiatively or collisionally. Thus, any excited state fluorescence observed in the late afterglow must have originated from the recombination of ions and electrons. Since the excited states formed depend only on the details of the recombination process and not on how the ions were originally produced, in the late afterglow the integrated optical emission is proportional to the number of ions formed in the excitation–ionization process.

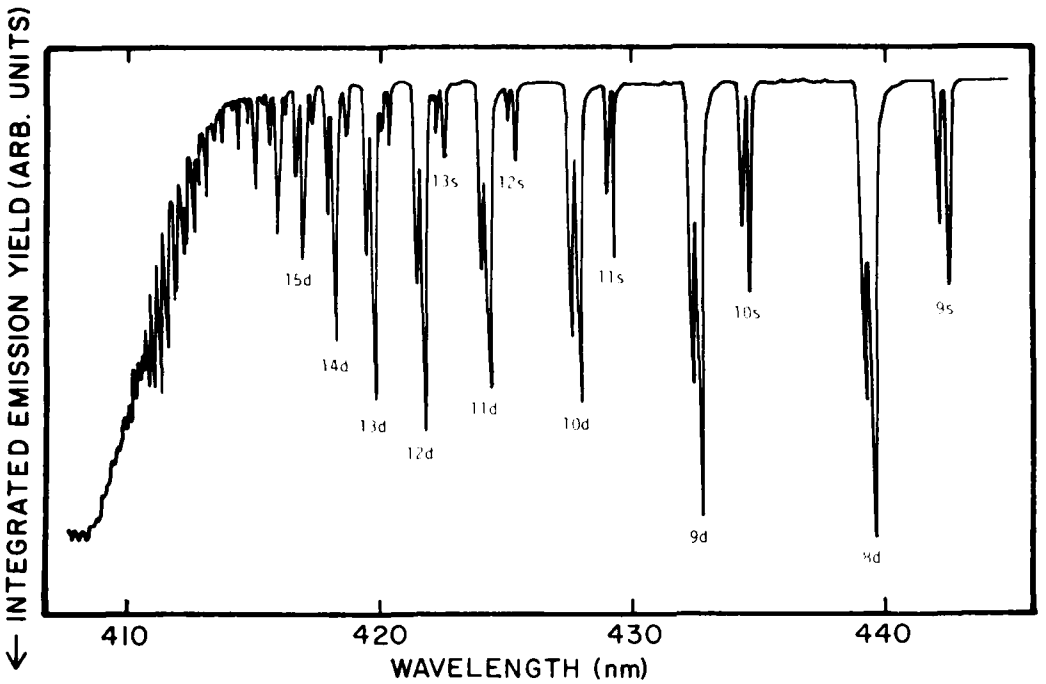

FIG. 5. Scan of fluorescence yield vs the wavelength of the second, ionizing laser. The ionization limit corresponds to a wavelength of 408 nm. Identical spectra are obtained if the ions/electrons are collected directly.

The excitation–ionization process leading to nearly complete ionization can be understood in terms of the electron-seeding model proposed by Measures and Cardinal.[2] In this model, the presence of a small number of seed electrons produced by photoionization and a densely populated excited state can lead to nearly saturated ionization. The reservoir of excited state atoms is a source of energy which can be transferred to the seed electrons in superelastic collisions. These energetic electrons can now excite and/or ionize the sodium. An excellent description of this process is given in Ref. 2.

If the second (blue) laser is tuned through a $3p$–nd (ns) transition, the number of seed electrons produced is proportional to the transition moment, the laser intensity, and the photoionization cross section of the nd (ns) state.[2] The seed electron density in turn deter-

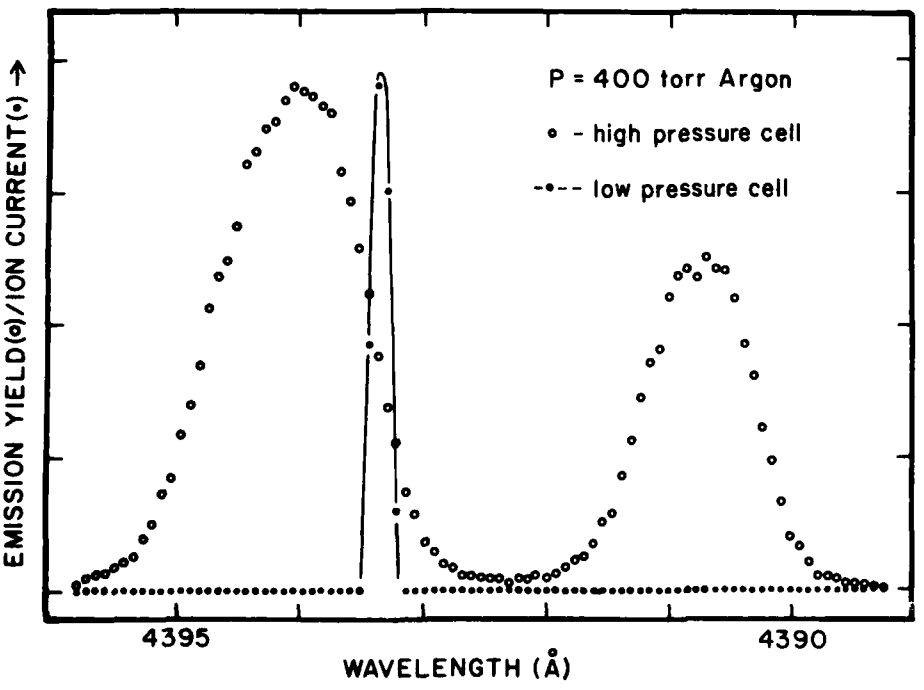

FIG. 6. Fluorescence yield vs laser wavelength for the $3p \rightarrow 8d$ transitions from a scan taken simultaneously in a cell with 400 Torr of argon buffer and a cell with no buffer gas. Two components are present in the high pressure cell due to collisional mixing of the $3\,^2P_{3/2,1/2}$ levels. Identical spectra are obtained if the ions/electrons are collected directly.

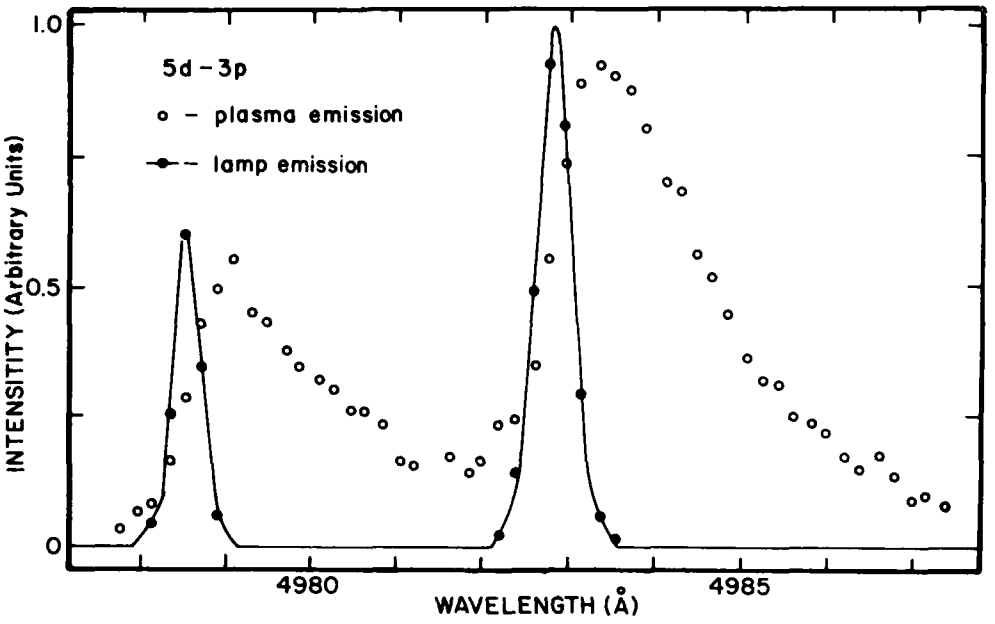

FIG. 7. Simultaneous high resolution scan of plasma emission and lamp emission.

mines the ultimate ion/electron density. If we observe the integrated emission from the interaction zone and scan the frequency of the second laser, we obtain the spectrum shown in Fig. 5. Since the excitation of the *nd* (ns) excited state takes place only during the 4 ns laser pulse, well before the ion/electron density reaches its peak (see Fig. 2), the shift of the spectral lines as observed while tuning the blue laser through a transition is *due only to the presence of the buffer gas*. A higher resolution tracing as the laser is scanned through the $3p-8d$ transition at 439 nm is shown in Fig. 6. The ion yield is recorded simultaneously in a cell with no buffer gas and a cell with 400 Torr of argon buffer. Two components appear in the high pressure scan representing the $3P_{1/2}$ and $3P_{3/2}$ levels which are collisionally mixed at the high buffer gas pressures. The shift in the emission lines due to the Ar buffer at 400 Torr is then simply determined.

2. *Pressure and electron density shifts*

The recombination spectrum shown in Fig. 3 is obtained by scanning the monochromator through the respective transitions with the synchronous photon counter set for a delay of 2 μs after the laser pulses and with an aperture of 1.0 μs. This delay corresponds to the maximum electron density, as indicated from Fig. 2. The emission lines are thus shifted (and broadened) both by collisions with electrons and the 400 Torr argon buffer. Figure 7 is a high-resolution monochromator scan of the $6d-3p$ transition under these conditions.

In Fig. 8, we show the shifts for the $3p-5d$, $6d$, and $7d$ transitions obtained by (a) scanning the second dye laser through the transition and (b) scanning the monochromator through the indicated transition. The difference in the shifts between the two curves is then due to the difference in the electron density under the two conditions.

D. Electron density from shift data

Line shifts in Na due to collisions with electrons have been computed theoretically by Griem.[7] In Fig. 9 the results obtained by Griem are extrapolated to 900 K and an electron density of 6.8×10^{14} cm^{-3} and shown as circles. A solid line connects the computed shifts to aid the eye. The square points are the experimental shifts we measure by the technique outlined in the preceding sections. A dotted line connects the experimental points. The 900 K electron temperature was derived from our Saha plots as described in Sec. III B. The 6.8×10^{14} cm^{-3} yields the best fit of the theoretical data of Griem to our experimental results.

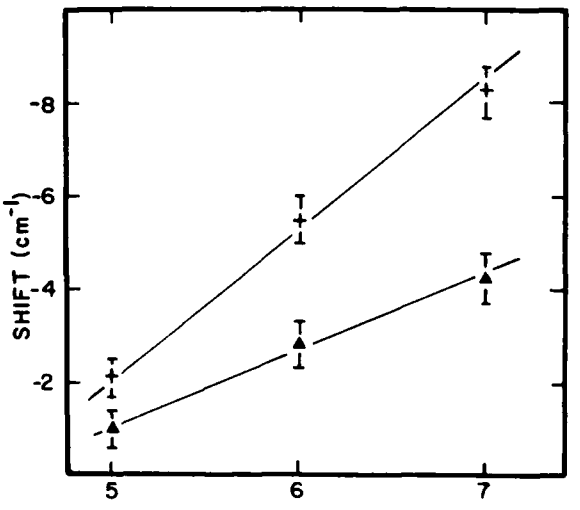

FIG. 8. Shift vs principal quantum number for $3\,^2P_{3/2}\rightarrow n\,^2D$ transitions, as determined from scans of the plasma emission (+) and absorption measurements (▲) with 0.43 amagat of argon buffer.

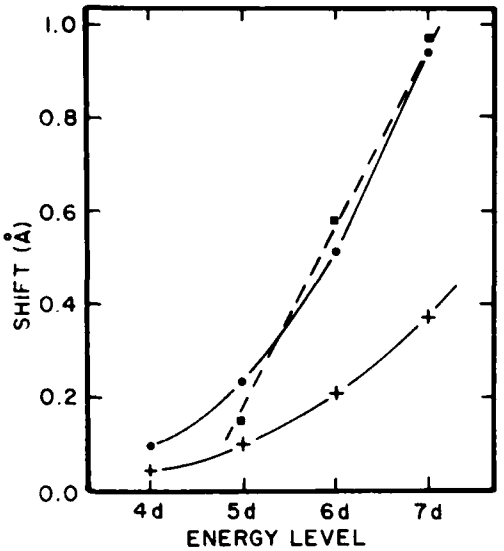

FIG. 9. Stark shift vs principal quantum number calculated by Griem for $T_e = 10\,000$ K, $n_e = 6.8\times10^{14}$ cm^{-3} (+), $T_e = 900$ K, n_e 6.8×10^{14} cm^{-3} (●); and experimental points (■).

E. Electron density measurements from charge collection

An electric field applied across the interaction region defined by the laser beams can be used to extract charge produced in the excitation–ionization process. At the electron densities of this experiment, the Debye shielding length is less than the diameter of the reaction region; consequently, the electric field does not penetrate completely into the line charge and only a small portion of the charge is collected by the electrodes. Those electrons that are removed from the interaction volume cannot, of course, participate in the recombination process.

The application of a 100 V/cm electric field to the interaction volume reduces the integrated recombination fluorescence by approximately 20%. Equating this reduction to the measured charge collected at the electrodes, we find that the electron density of the laser-induced plasma is 3×10^{14} cm^{-3}.

The results obtained in this section are intended to be suggestive only and are included only because the electron densities obtained agree within reasonable expectations with the electron density measurements obtained from the line shift data and the Saha–Boltzmann plots.

TABLE I. Electron density measurements.

Electron density (cm^{-3})	Method
3.4×10^{14}	Saha–Boltzmann plot
4.1×10^{14}	Stark shift ($5d\rightarrow3p$)
7.1×10^{14}	Stark shift ($6d\rightarrow3p$)
7.0×10^{14}	Stark shift ($7d\rightarrow3p$)
3.0×10^{14}	Charge extraction

IV. SUMMARY

The electron density in a laser-excited Na plasma at high buffer gas pressures has been measured in three different ways: (1) Saha–Boltzmann plots, (2) spectral line shifts due to electron collisions, and (3) charge extraction.

The results are summarized in Table I. The laser excitation and cell conditions are identical in each case. The Saha plots depend upon an absolute calibration of the detection system to determine the electron density and is reliable only to within a factor of 3. The electron temperature, however, depends only a relative calibration which is accurate to 10%. The electron density measurement from the charge extraction depends on some assumptions which appear to be reasonable but could not be independently verified.

Thus, despite the variation in the measured electron densities shown in Table I, we regard the different methods of obtaining the electron density as yielding satisfactory results. Both methods 1 and 2 are noncontact, nonperturbative methods. The spectral line shifts are, however, far easier to determine with good precision.

[1](a) T. B. Lucatorto and T. J. McIlrath, Phys. Rev. Lett. **37**, 428 (1976); (b) T. J. McIlrath and T. B. Lucatorto, *ibid.* **38**, 1390 (1977).
[2]R. M. Measures and P. G. Cardinal, Phys. Rev. A **23**, 804 (1981).
[3]G. H. Bearman and J. J. Levanthal, Phys. Rev. Lett. **41**, 1227 (1978).
[4]M. Allegrini, G. Alzetta, A. Kopystynska, L. Moi, and G. Orriols, Opt. Commun. **19**, 96 (1976).
[5]D. Krebs and L. D. Schearer, J. Chem. Phys. **75**, 3340 (1981).
[6]J. F. Kielkopt and R. B. Knollenburg, Phys. Rev. A **12**, 559 (1975).
[7]H. R. Griem, *Plasma Spectroscopy* (McGraw–Hill, New York, 1964).

END

FILMED

7-84

DTIC